THE JOURNAL OF PHYSICAL CHEMISTRY C

Article

pubs.acs.org/JPCC

Femtosecond to Microsecond Dynamics of Soret-Band Excited Corroles

Sai Santosh Kumar Raavi,*[,†,‡,§] Jun Yin,[‡] Giulia Grancini,[§] Cesare Soci,[‡] Venugopal Rao Soma,[∥] Guglielmo Lanzani,[§] and Lingamallu Giribabu[⊥]

[†]Department of Physics, Indian Institute of Technology Hyderabad, Kandi, Sangareddy 502285, Telangana, India

[‡]School of Physical and Mathematical Sciences, Nanyang Technological University, 21 Nanyang Link SPMS-04-01, Singapore 637371

[§]Center for Nanoscience and Nanotechnology@PoliMi, Istituto Italiano di Tecnologia, Via Pascoli 70/3, Milan, Italy

[∥]Advanced Centre of Research in High Energy Materials (ACRHEM), University of Hyderabad, Hyderabad 500046, Telangana, India

[⊥]Inorganic and Physical Chemistry Division, CSIR-Indian Institute of Chemical Technology, Hyderabad 500007, India

Supporting Information

ABSTRACT: We present a comprehensive photophysical investigation on a series of three corroles (TTC, P-TTC, Ge-TTC dissolved in toluene), employing femtosecond and nanosecond transient absorption spectroscopy (TAS) measurements. Systematic analyses of the TAS data determined the rates and corresponding time constants of photophysical processes: internal conversion (τ_{IC}) in the 898−525 fs range, vibrational relaxation in the 7.44−13.6 ps range, intersystem crossing in the 033−1.09 ns range, and triplet lifetime ($\tau_{triplet}$) in the 0.8−3.5 μs range. The estimated triplet quantum yields ($\Phi_{triplet}$) were in the 0.42−0.61 range. Comparatively, GeTTC displayed faster τ_{IC} and higher $\Phi_{triplet}$. Additionally, the time-dependent density functional theory calculations were performed for the three molecules. The HOMO/LUMO energy levels and the oscillator strengths of various transitions were determined and presented.

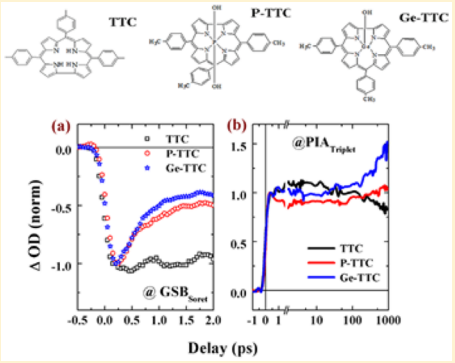

INTRODUCTION

The chemistry and photophysics of normal porphyrins have been profoundly explored, in large part, due to their relevance to biological active sites and as components of advanced devices.[1] The optical, electronic, and nonlinear optical (NLO) properties of porphyrins are well-documented in the literature.[2−4] This has opened new avenues for studies on similar macrocycles or porphyrinoids, such as corroles, core-modified rings, etc., for the past couple of decades. Corrole macrocycle is a contracted analogue of a porphyrin in which one meso position has been eliminated yet still possessing the 18 π-electron aromaticity of porphyrins.[5] The structure of a corrole molecule represents an intermediate between porphyrin and the corrin ring in the B12 cofactor. The first investigation on corrole was performed by Johnson and Kay in the late 1960s when the macrocycle was produced as a byproduct during the synthesis of B12.[6,7] While corroles have been known for more than 40 years, research progress in this field was slow. However, investigations on corroles have recently increased with the synthetic work of the groups of Paolesse and Gross, who reported one-pot synthesis of triaryl corroles. This provided a new impetus to the synthesis of new corrole molecules with emphasis, particularly, on the peripheral functionalization of the macrocycle.[8,9]

Unlike porphyrins, corroles are tris-anionic ligands that stabilize unusual high oxidation states of metal centers like Fe(IV), Cu(III), Au(III), Mn(V), Ge(IV), Sn(IV), P(V), etc.[10] When compared to porphyrins, corroles are tribasic aromatic macrocycles exhibiting interesting properties such as lower oxidation potentials, higher fluorescence quantum yields, larger Stokes shift, and relatively more intense absorption.[11−13] The typical corrole absorption consists of an intense Soret band in blue region, due to $\pi-\pi^*$ electronic transition from ground state to the higher excited state (S_n) and three less intense Q bands in red region, originating from $n-\pi^*$ electronic transitions, attributed to the first excited state (S_1), yet they lack significant optical cross sections for a large portion of the visible spectrum (450−550 nm). The versatile spectral, electrochemical, and photophysical properties of corroles make them suitable for potential applications[14−25] in photodynamic therapy (PDT), cancer diagnosis, molecular catalysis, oxidation, reduction, and group transfer reactions of many organic transformations, photosensitizers for organic solar cells, fluorescence imaging agent, etc. Furthermore, the electron-rich π-system has generated strong interest for the study of NLO properties of these corroles for potential applications in data storage, optical limiting, multiphoton absorption, fluorescence, and surface-enhanced Raman scattering.[26−34] Therefore, investigation of photophysical properties of corroles is indispensable for identifying the true potential of these

Received: August 24, 2015
Revised: November 6, 2015
Published: December 2, 2015

DOI: 10.1021/acs.jpcc.5b08235
J. Phys. Chem. C 2015, 119, 28691−28700

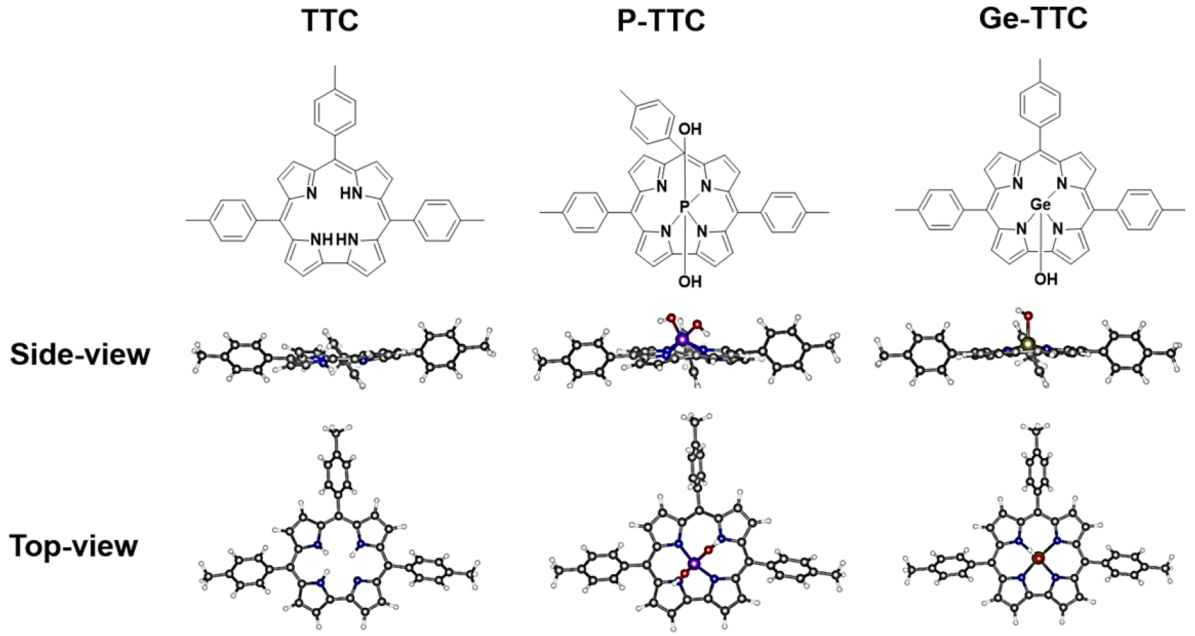

Figure 1. Molecular structures and optimized structural geometries of TTC, P-TC, and Ge-TTC with side and top views.

macrocycles in a variety of applications. Furthermore, the knowledge of these properties is imperative for designing efficient corrole-based materials for optoelectronic and solar cell applications. There have been a few photophysical studies of corroles reported in terms of structure−function relationships such as interpretation of photophysics as a function of meso-substituion,[30,35−38] β-substituted free-base corroles,[39] metalated corroles,[40] N−H tautomerization,[41,42] higher order architectures such a corrole−fluorophore dyads,[43,44] corrole−porphyrin dyads,[45,46] etc.

In this communication, we present results from the investigation of photophysical properties of three corrole molecules, namely, (a) 5,10,15-tris(4-methyl phenyl) corrole (herewith referred to as TTC) and (b) its phosphorus(V) and (c) germanium(IV) metallo derivatives (herewith referred to as P-TTC and Ge-TTC, respectively) using time-dependent density functional theory (TD-DFT) calculations and transient absorption spectroscopy (TAS) studies in the femtosecond to microsecond time scales along with steady-state absorption and fluorescence spectroscopy techniques.

COMPUTATIONAL METHODS

Density functional theory (DFT) was implemented to understand and interpret the electronic and optical properties of corroles. The geometries of neutral, charged, and triplet state of these molecules were optimized by restricted or unrestricted functional B3LYP, together with basis sets 6-31G(d, p). The solvent effects, toluene used in the absorption spectra measurements, were taken into account with the conductor-like polarizable continuum model (CPCM). All the optical transitions and corresponding excitation energies and oscillator strength of neutral and charged state were calculated by TD-DFT method under the same hybrid functional and basis set. All the calculations were done with Gaussian09 program (Revision B.01).

EXPERIMENTAL DETAILS

The corroles investigated here are synthesized and purified using standard procedures. The synthesis procedures are reported elsewhere (TTC,[47] P-TTC,[45] Ge-TTC[46]). Their respective molecular structures are presented in Figure 1. Spectroscopic grade anhydrous toluene was used as the solvent to prepare dilute solutions of 10 μM concentration to avoid any aggregation affects. Prepared solutions are degassed with continuous flow of nitrogen gas for 2 h. The degassed solutions are filled into quartz cuvettes (Hellma110-QS) of 1 mm optical path length and kept sealed for all the spectroscopy measurements. The steady-state absorption and emission spectra measurements were performed using a LAMBDA-1050 spectrophotometer (PerkinElmer) and Nanolog spectrofluorimeter (Horiba Jobin Yvon), respectively.

Femtosecond transient absorption (fs-TA) measurements were performed using a commercial Ti:Sapphire regenerative amplifier (Quantronix model Integra-C), delivering 1 kHz, ∼1 mJ pulses at a central wavelength of 800 nm and ∼150 fs duration. Complete details of the experimental setup are reported and described in our earlier works.[48] In the present work we used second harmonic of the fundamental pulses centered at 400 nm as the pump to resonantly excite sample in the Soret band. Another small fraction (∼2 μJ) of the amplifier output was independently focused into a 1 mm thick sapphire plate to generate a stable single-filament white-light super continuum that served as the probe. By utilizing a filter the probe spectral window was limited to the 415−760 nm spectral range. The normalized transmission change $\Delta T/T$ is measurement using a pump−probe setup consisting of a computer-controlled optical multichannel analyzer, which enabled single-shot detection at 1 kHz repetition rate. The instrument response was estimated to be ∼220 fs. The data were recorded to the pump−probe delay window of −2 ps to +1.2 ns. Pump pulses with typical energies of 200 nJ per pulse were used for the measurements. All the measurements were performed at room temperature.

DOI: 10.1021/acs.jpcc.5b08235
J. Phys. Chem. C 2015, 119, 28691−28700

Nanosecond transient absorption (ns-TA) measurements were performed with a LP920 laser flash spectrometer (Edinburgh Instruments). It is based on a standard "pump−probe" setup where the sample is excited by a nanosecond laser pulse (pump), and the time evolution of the differential absorption changes (ΔOD) induced by the pump is monitored by a second weak probe generated by a CW light source. The pump pulses centered at 410 nm were provided by a tunable nanosecond OPOLett-355II laser (10 Hz repetition rate). The probe light was provided by a pulsed Xenon arc lamp. The sample was kept at 45° to the excitation beam. The beams were focused onto the sample ensuring the spatial overlap. The transmitted probe was spectrally filtered by a monochromator and detected. A set of photomultipliers (with both visible and near-IR detection window) enabled the collection of single-wavelength kinetics with superior sensitivity. The signal (ΔOD) was then recorded using a TDS 3032C digital signal analyzer.

RESULTS AND DISCUSSION

Steady-State Spectra. The steady-state absorption spectra of TTC, P-TTC, and Ge-TTC in toluene are shown in Figure 2

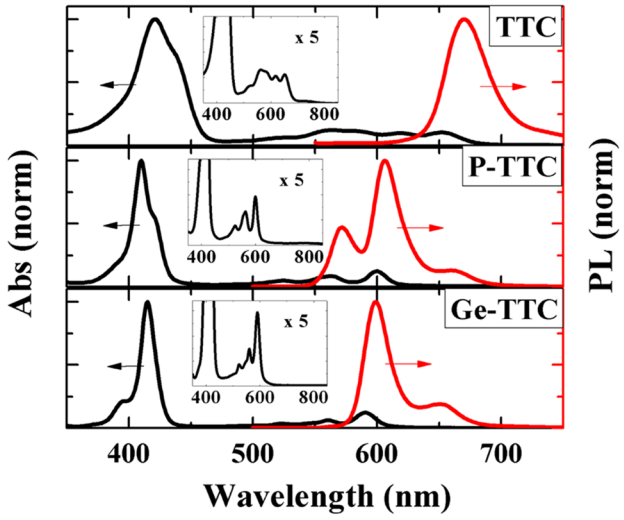

Figure 2. Absorption spectra (black curves) and PL spectra (red curves) of TTC, P-TC, Ge-TTC. (inset) The 5× enlargement of the weak Q-band absorption.

(black curve). An intense and broad band near 420 nm (Soret), due to strong $\pi-\pi^*$ electronic transitions, was observed. P-TTC and Ge-TTC illustrated stronger Soret absorption with sharper absorption peaks compared to the free base corrole TTC. The inset shows the magnified (5×) Q-bands that are due to the $n-\pi^*$ electronic transitions contributing to weaker absorption bands in the visible region (500−700 nm). The steady-state emission of the corroles was recorded with 400 nm excitation. P-TTC and Ge-TTC data depicted strong blue-shifted emission with distinct vibronic features compared to TTC. In corroboration with our earlier report,[32] we noticed that the strongest emission was observed from the P-TTC molecule. Particularly, the photoluminescence (PL) spectra demonstrated a negligible Stokes shift at the Q-band absorption edge for all three corroles investigated. The coefficients obtained from the steady-state measurements are summarized in Table 1. The fluorescence quantum yields and the lifetime data were obtained from our earlier measurements.[32]

Quantum Chemistry Calculations. Figure 1 depicts the optimized geometry of molecule TTC, and it was observed to be nonplanar due to the steric hindrance between neighboring hydrogen atoms at the central core and twisted methylbenzene with dihedral angle of ∼12°. Substitution of P atom at the central core for P-TTC exhibited a further distortion in the tetrahedral geometry.[49] Substitution of Ge in the central core for Ge-TTC made the central geometry almost flat with the small dihedral angle of ∼3°. Figure 3 illustrates the results of

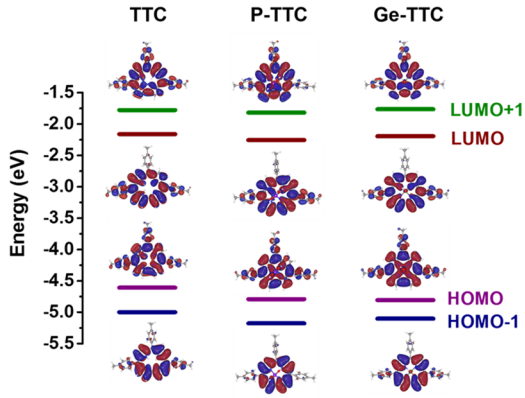

Figure 3. Frontier molecular orbital energies and electronic density distribution of molecules TTC, P-TTC, and Ge-TTC.

DFT calculations for the electronic density distribution of frontier orbitals for the molecules as well as their corresponding frontier molecular orbital energies. From the data presented in Figure 3 we observed that for TTC the electronic distribution of highest occupied molecular orbital (HOMO) depicts π-bonding character, spreading over the whole molecule, and lowest unoccupied molecular orbital (LUMO) shows π^*-antibonding character being predominately localized on the central core and two of sided methylbenzene units. Both P-TTC and Ge-TTC retain the electronic characterization of TTC but with additional electronic distribution along P−OH and Ge−OH bonds. The introduction of heteroatoms into the TTC core reduced the frontier orbital energies, especially for P-TTC, due to strong electron-accepting −OH groups. The calculated optical transitions from singlet ground state (S_0) to upper excited states (S_n) are plotted in Figure S1 (left side).

Table 1. Summary of Absorption and Fluorescence Peaks[a] of the Three Corroles in Toluene Recorded at Room Temperature

	absorption peaks [nm]						
sample	Soret band [ε (M^{-1} cm^{-1})]	Q-band [ε (M^{-1} cm^{-1})]			emission λ_{max} (nm)		
TTC	421 [106 465]	564 [13 079]	619 [10 577]	650 [106 465]		670	
P-TTC	410 [154 828]	524 [7761]	563 [13 348]	600 [19 264]	570	605	665
Ge-TTC	415 [238 894]	524 [8555]	561 [14 849]	591 [29 403]	600		650

[a]The values in parentheses represent the extinction coefficient (ε, in M^{-1} cm^{-1}).

DOI: 10.1021/acs.jpcc.5b08235
J. Phys. Chem. C 2015, 119, 28691−28700

Our calculated spectra obtained using TD-DFT method including solvent effects was in good agreement with the experimental steady-state absorption data presented in Figure 2. The first weak broad band in the 540−580 nm range is from the $S_0 \rightarrow S_1$ transition with dominant contribution of HOMO → LUMO. We observed very weak oscillator strength for $S_0 \rightarrow S_2$. The most intense peak at 426, 406, and 400 nm for TTC, P-TTC, and Ge-TTC, respectively, is found to be from $S_0 \rightarrow S_4$ transition with main contribution of HOMO−1 → LUMO+1. These peaks are in good agreement with the experimental Soret bands. The detailed calculations of the optical transitions are presented in Table 2.

Table 2. Summary of Orbital Transitions Calculated by TDDFT for the Lowest Singlet Excited Electronic States of TTC, P-TTC, and Ge-TTC

molecule	orbital transitions	wavelength (nm)	oscillator strength	major contributions
TTC	$S_0 \rightarrow S_1$	588	0.32	HOMO−1 → LUMO +1 (14%)
				HOMO → LUMO (78%)
	$S_0 \rightarrow S_2$	540	0.05	HOMO−1 → LUMO (44%)
				HOMO → LUMO+1 (47%)
	$S_0 \rightarrow S_3$	423	1.21	HOMO−1 → LUMO (50%)
				HOMO → LUMO+1 (47%)
	$S_0 \rightarrow S_4$	410	1.49	HOMO−1 → LUMO +1 (81%)
				HOMO → LUMO (14%)
P-TTC	$S_0 \rightarrow S_1$	566	0.30	HOMO−1 → LUMO +1 (11%)
				HOMO → LUMO (77%)
	$S_0 \rightarrow S_2$	536	0.06	HOMO−1 → LUMO (44%)
				HOMO → LUMO+1 (44%)
	$S_0 \rightarrow S_3$	415	1.01	HOMO−1 → LUMO (45%)
				HOMO−1 → LUMO +1 (9%)
				HOMO → LUMO+1 (43%)
	$S_0 \rightarrow S_4$	396	1.30	HOMO−1 → LUMO +1 (74%)
				HOMO → LUMO (12%)
Ge-TTC	$S_0 \rightarrow S_1$	549	0.30	HOMO−1 → LUMO +1 (17%)
				HOMO → LUMO (83%)
	$S_0 \rightarrow S_2$	518	0.004	HOMO−1 → LUMO (57%)
				HOMO → LUMO+1 (43%)
	$S_0 \rightarrow S_3$	401	1.30	HOMO−1 → LUMO (42%)
				HOMO → LUMO+1 (57%)
	$S_0 \rightarrow S_4$	397	1.38	HOMO−1 → LUMO +1 (81%)
				HOMO → LUMO (17%)

Femtosecond and Nanosecond Transient Absorption Data. The fs-TAS measurements were performed with 400 nm photoexcitation in the Soret band, and the data were collected up to a delay of 1.2 ns. Considering the TD-DFT calculations we construed that the photoexcitation takes place to S_4 state for all the molecules. Investigation of ultrafast excited-state dynamics revealed crucial insight into the ultrafast internal conversion (IC) from $S_4 \rightarrow S_1$ followed by the vibrational relaxation (VR) within S_1. From the ns-TAS measurements the excited-state evolution, specific to the triplet state decay and in the time window of 6 ns to a few microseconds was recorded. Thus, by combining the two techniques the photoexcited population was monitored from the initial S_4 state until it decayed completely to the ground state.

Figure 4 shows the TA spectra for TTC, P-TTC, and Ge-TTC in toluene solution. The obtained spectra revealed that

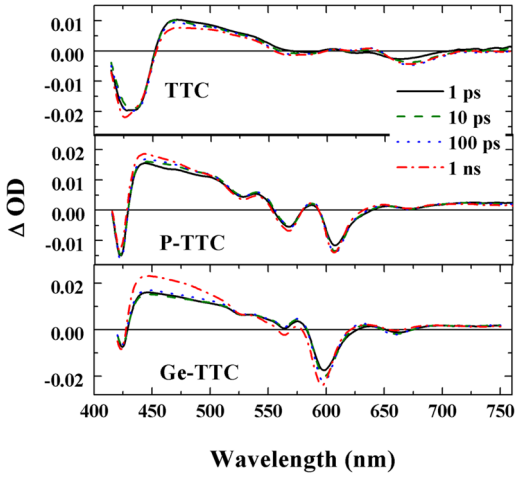

Figure 4. fs-TA spectra of TTC, P-TC, and Ge-TTC recorded at 1 ps, 10 ps, 100 ps, and 1 ns.

the data possessed three distinct regions: (i) a negative band in the 415−440 nm spectral region representing the ground-state bleach (GSB_{soret}) due to the Soret-band absorption, (ii) a positive spectral band in the 430−570 nm spectral region demonstrating a photoinduced absorption (PIA) representing the overlap excited state absorption spectra of singlet as well as triplet species, and (iii) a negative band in the 570−700 nm spectral region representing an overlap of $GSB_{Q\text{-band}}$, due to the weaker Q-band absorption and the stimulated emission (SE), which was due to PL of the molecules in the same spectral region. The SE maxima were observed in the vicinity of 670, 605, and 600 nm for TTC, P-TTC, and Ge-TTC, respectively, which are also their PL maxima. The vibronic features of the Q-band absorption can be seen from these TA spectra overimposed with the dominant PIA and SE in the 500−650 nm region. The GSB in the 400−450 nm range displayed a broad negative TA with maximum near 430 nm for TTC, while the negative TA maximum was observed near 425 for both P-TTC and Ge-TTC. This is in agreement with the spectral narrowing, blue-shift observed in the absorption with the substitution of P and Ge atoms. Since the probe spectral window was limited to 415 nm the lower spectral region of the GSB from P-TTC and Ge-TTC could not be recorded. The positive PIA maximum for TTC was observed at 470 nm (at 1 ns) suggesting the peak of the long-lived TA signal from triplet−triplet state absorption. Similarly, the PIA maxima were

DOI: 10.1021/acs.jpcc.5b08235
J. Phys. Chem. C 2015, 119, 28691−28700

observed at 450 and 445 nm for P-TTC and Ge-TTC, respectively, at 1 ns pump−probe delay. The strength of the PIA was strong for Ge-TTC compared to P-TTC and TTC (in that order) indicating that the yield of triplets in Ge-TTC to be the highest compared to the other two corroles.

A careful analysis of the TA data in the first 50 ps after photoexcitation offered insight into the internal conversion (IC) from $S_4 \rightarrow S_1$ and the vibrational relaxation (VR) mechanisms within S_1 for the considered corroles. Figure 5

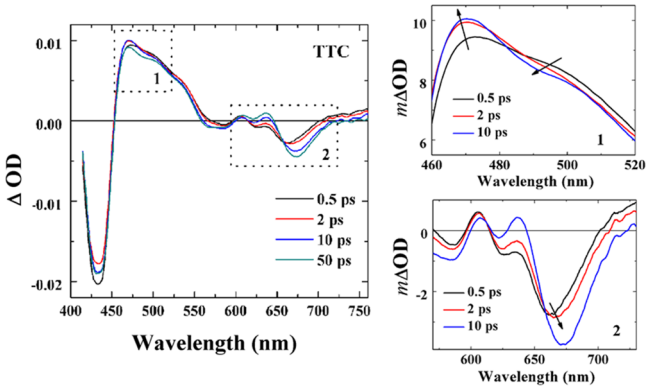

Figure 5. (left) fs-TA spectra of TTC showing the spectral evolution from 0.5 to 50 ps; (right) enlargement of the PB (region 1) and PA (region 2).

illustrates the spectral evolution obtained for TTC. The left panel displays the TA spectra recorded at 0.5, 2, 10, and 50 ps. Two spectral windows (regions 1 and 2) are chosen to describe the spectral changes with time. The right panel shows the enlarged image of the selected regions. In region 1, spectral evolution of the PIA band is illustrated. The peak near 490 nm decayed within the first 2 ps with simultaneous growth of the peak in the vicinity of 470 nm, until 10 ps. However, region 2 depicts the negative band (SE+ $GSB_{Q\text{-band}}$). The negative maxima near 470 nm (corresponding to SE) illustrated a gradual red shift in 10 ps. The growth of this SE band may be due to the decay of the competing PIA process and gradual increase of the population of S_1 state. The red shift of the SE peak also indicates the relaxation from a higher (hot) vibrational state to lower vibrational state. At the same time, the peak near 640 nm changed from negative to positive. From the data presented in two regions it can be construed that the TA spectral evolution until the first 2 ps and the spectra thereafter belongs to two distinct excited species. Considering the Soret-band photoexcitation, the primary photoevent should be the IC bringing the excited population to the highest vibrational level of S_1 within of first 2 ps. From the data presented in the left panel of Figure 5 it is evident that the TA spectra at 10 and 50 ps had no significant change in the spectral shape suggesting that they are from the same excited species. The relaxation within the vibrational levels of S_1 [referred to as the VR] is completed within 10 ps. Similar analysis for the other two corroles is provided in the Supporting Information (Figures S2 and S3). For Ge-TTC the IC happens at a much faster scale, while the VR slowed down, perhaps, due to the heavier molecular weight.

Figure 6 presents the TA kinetic profiles recorded at selected wavelengths for TTC along with the best fit obtained using the global fit analysis described in the later part of this section. The displayed wavelengths were chosen to represent the various

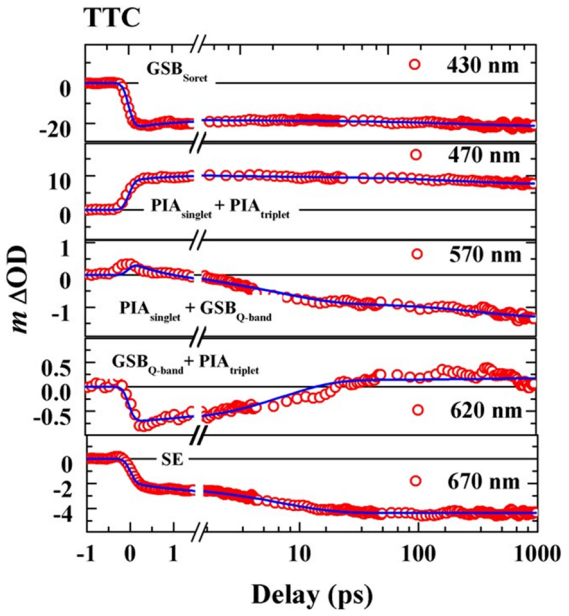

Figure 6. TA kinetics of TTC at selected probe wavelengths. (red ○) Experimental data. (blue) Theoretical fits after global analysis.

photo processes observed. The kinetics of the negative GSB_{Soret} at 430 nm represents Soret-band absorption. We noticed the TA at 430 nm did not decay until the end of the pump−probe delay suggesting the formation of long-lived excited states, which results in the loss of population in the ground state (S_0). From our DFT analysis we identified the formation of triplet states, which are usually long-lived. A quick look at the TA spectra, illustrated in Figure 4, points out the complicated spectral and kinetic evolution of the PIA band. Significantly, the PIA band did not have distinct signatures for singlet and triplets. It is well-established that the higher singlet states are short-lived, while the triplet states are long-lived. As a representative of the PIA band, the maxima peak at 470 nm was chosen for analysis. We observed the TA kinetics lived long as well and formed at the earliest delay after the photoexcitation. Thus, we concluded the band consisted of PIA from both singlets as well as triplet states. From our earlier analysis, we concluded that initial kinetics (until the first 50 ps) was due to PIA from singlets, and there we observed the onset of long-lived triplet state absorption. The strongest peak of the Q-band absorption was near 570 nm. We expected the TA kinetics at this wavelength to be negative ($GSB_{Q\text{-band}}$). However, the initial kinetics until 2 ps was positive pointing to the presence of competing PIA, probably from the higher singlet states. Subsequently, we observed a gradual formation and growth of the negative $GSB_{Q\text{-band}}$ suggesting a weak $PIA_{singlet}$ and, may be, much weaker or no $PIA_{triplet}$ in this spectral region and a dominant $GSB_{Q\text{-band}}$. At 620 nm, where the Q-band has its second maxima, there was immediate formation of $GSB_{Q\text{-band}}$, which gradually decayed and changed to PIA after 10 ps. The PIA formation is complete at ∼500 ps suggesting the strong formation of triplets on that time scale. The SE kinetics was observed at 670 nm, which is the PL maximum of TTC. We observed a monotonous growth here, as expected.

From the emission data presented in Figure 2 we noticed a strong blue shift of Q-band absorption, and PL was observed for Ge-TTC and P-TTC compared to TTC. Therefore, the TA kinetics of representative wavelengths from Q-band and SE for

DOI: 10.1021/acs.jpcc.5b08235
J. Phys. Chem. C 2015, 119, 28691−28700

P-TTC and Ge-TTC is expected to demonstrate a different behavior to that observed in TTC. The TA kinetics of P-TTC and Ge-TTC are presented in Figures 7 and 8, respectively.

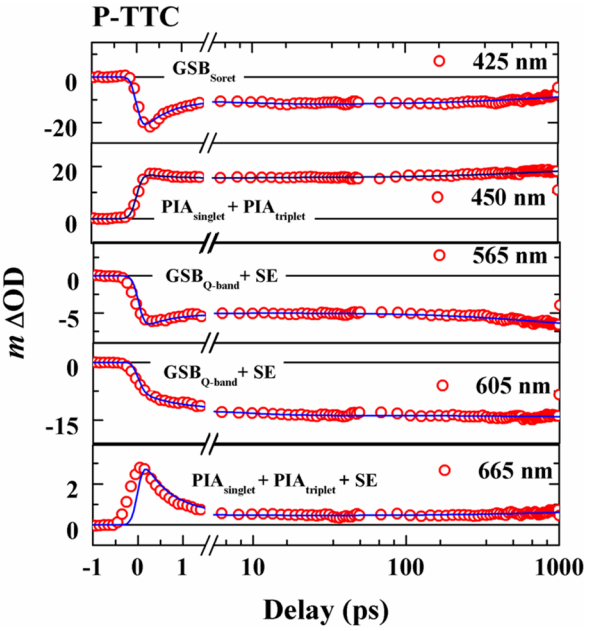

Figure 7. TA kinetics of P-TTC at selected probe wavelengths. (red ○) Experimental data. (blue) Theoretical fits after global analysis.

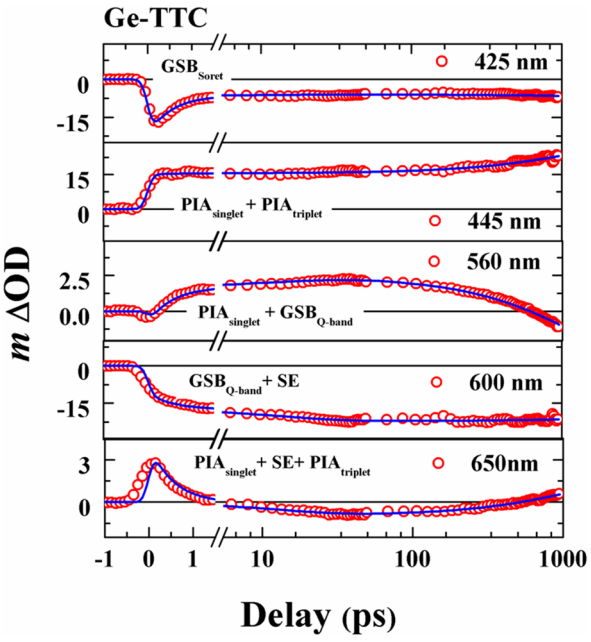

Figure 8. TA kinetics of Ge-TTC at selected probe wavelengths. (red ○) Experimental data. (blue) Theoretical fits after global analysis.

The kinetics at 425 nm, corresponding to GSB_{Soret} for both the corroles and the PIA peak for P-TTC at 450 nm and Ge-TTC at 445 nm, depicted long lifetime similar to what was observed with TTC. For both P-TTC and Ge-TTC we observed the contribution of dominant SE along with $GSB_{Q\text{-band}}$ at 605 nm, which were also their PL maxima and Q-band absorption maxima. The kinetics of P-TTC at 565 and 665 nm portrayed a different trend contrary to the expected logic and is evident from the data presented in Figure 7. The kinetics at 565 nm was observed to be negative and long-lived, which is expected since there is a spectral overlap of Q-band and PL, and therefore, both $GSB_{Q\text{-band}}$ and SE contribute to the TA kinetics. For 665 nm kinetics, where one expects a long-lived SE signal, we observed a negative signal that can be attributed to be a resultant of competition from the dominant PIA. In the same vein, the kinetics of Ge-TTC at 560 and 650 nm displayed an unexpected trend, where we concluded the temporal profile of 560 nm is a resultant of $PIA_{singlet}$ and $GSB_{Q\text{-band}}$ and the 650 nm kinetics to be a resultant of $PIA_{singlet}$, SE and $PIA_{triplet}$. With substitution of heavier atom in the central core we observed a faster IC and higher triplet yield. Figure 9a confirms the faster

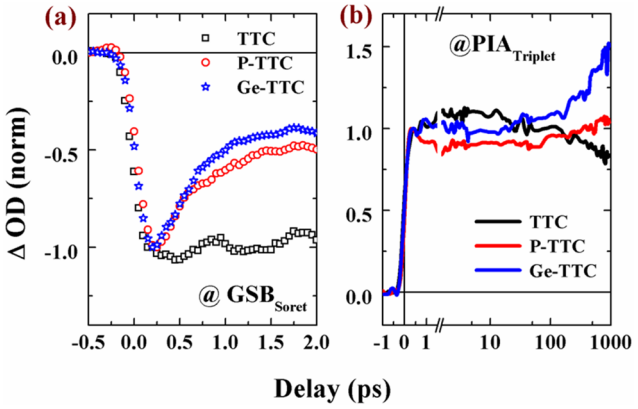

Figure 9. Comparison of normalized TA kinetics at (a) peak of PB near Soret band absorption (425 nm) and (b) peak of triplet band for TTC (470 nm), P-TTC (450 nm), and Ge-TTC (445 nm).

IC process from $S_4 \rightarrow S_1$ upon comparing the normalized TA kinetics of GSB_{Soret} for the three corroles until the first 2 ps. At longer time delays (~1 ns) we observed the growth in the positive $PIA_{triplet}$ kinetics for Ge-TTC higher than P-TTC, which is more than TTC as shown in Figure 9b. This indicated the triplet yield was highest for Ge-TTC.

Following the fs-TAS measurements, where we observed the PIA peak to be at 470, 450, and 445 nm for TTC, P-TTC, and Ge-TTC, respectively, we measured the ns-TA kinetics in the same wavelengths. Figure 10 illustrates the ns-TA kinetics for the three corroles along with the monoexponential decay fit to

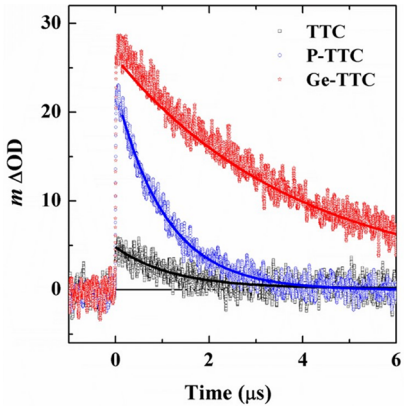

Figure 10. ns-TA kinetics at the peak of triplet band for TTC (470 nm, black), P-TTC (450 nm, blue), and Ge-TTC (445 nm, red). Scattered points represent the experimental data, while the solid lines are the exponential fits.

DOI: 10.1021/acs.jpcc.5b08235
J. Phys. Chem. C 2015, 119, 28691−28700

Table 3. Summary of Global Fit Parameters[a] of fs-TAS Measurements and Triplet State Parameters Obtained from Both fs-TAS and ns-TAS Experiments

	fs-TAS measurements				triplet state parameters		
sample	k_{IC} (s^{-1}) (τ_{IC})	k_{VR}(s^{-1}) (τ_{VR})	k_{ISC}(s^{-1}) (τ_{ISC})	$k_{triplet}$ (s^{-1})	$\tau_{triplet}$ (μs)	$\varepsilon_{triplet}$ (M^{-1} cm^{-1})	$\Phi_{triplet}$
TTC	1.11×10^{12} (898 fs)	1.34×10^{11} (7.44 ps)	3.01×10^{9} (0.33 ns)	1.21×10^{6}	0.82	38 671	0.43
P-TTC	1.57×10^{12} (636 fs)	1.43×10^{11} (6.95 ps)	1.09×10^{9} (0.91 ns)	1.13×10^{12}	1.03	68 072	0.58
Ge-TTC	1.91×10^{12} (525 fs)	7.33×10^{10} (13.6 ps)	9.98×10^{8} (1.09 ns)	1.13×10^{12}	3.50	77 760	0.61

[a] τ_{IC}, τ_{VR}, and τ_{ISC} represent the lifetimes of internal conversion, vibrational relaxation, and intersystem crossing, respectively.

estimate the lifetime of the triplet state. Since the concentration and the intensity of the excitation laser pulse were kept constant for all the measurements, these data reconfirm that Ge-TTC had the largest triplet yield. The estimated triplet lifetimes were 3.51, 1.03, and 0.82 μs for Ge-TTC, P-TTC, and TTC, respectively.

The triplet−triplet molar absorption coefficient $\varepsilon_{triplet}$ of the three corroles in toluene can be estimated using the eq-1:

$$\varepsilon_{triplet} = \varepsilon_{singlet}\frac{\Delta OD_{triplet}}{\Delta OD_{singlet}} \quad (1)$$

where $\Delta OD_{triplet}$ and $\Delta OD_{singlet}$ are the transient absorption change at the maximum of the positive PIA band and the minimum of GSB_{Soret} band, respectively, and $\varepsilon_{singlet}$ refers to the steady-state molar absorption coefficient at the minimum of GSB band. To this we chose the TA spectra recorded at 1 ns pump−probe delay, since at this delay we expect a majority population in the triplets manifold. Using the estimated $\varepsilon_{triplet}$, we evaluated the triplet quantum yields $\Phi_{triplet}$ for the three corroles according to the eq 2 (relative actinometry method)[50]

$$\Phi_{triplet} = \Phi_{singlet(std)}\frac{\Delta OD_{triplet}}{\Delta OD_{triplet(std)}}\frac{\varepsilon_{triplet(std)}}{\varepsilon_{triplet}} \quad (2)$$

Here, tetraphenylcorrole (TPC) was employed as the standard molecule for comparison ($\Phi_{triplet(std)}$ = 0.36).[37] We recorded the TA spectra for TPC in toluene at 1 ns (see the Supporting Information for details) and estimated $\varepsilon_{triplet(std)}$ using the eq-1. The estimated $\Phi_{triplet}$ values were 0.43, 0.58, and 0.61 for TTC, P-TTC, and Ge-TTC, respectively. All the estimated triplet state parameters are summarized in Table 3.

Global Fitting. The kinetics in such molecules is complicated mainly due to the overlapping contribution from several excited species. This is mainly because the measured transient absorption signal strength depends both on pump−probe delay and on the probe frequency ν; at each frequency (wavelength) the signal is the result of the overlap of several transitions, each weighed with its corresponding absorption cross section. From the observed data we propose the following explanation for sequence of events (i) following photo-excitation with 400 nm the population is driven directly into the higher singlet states, (ii) through internal conversion process the population reaches the highest (hot) vibrational levels of S_1state (denoted by S_1^*), (iii) the population then relaxes to the lowest vibrational level of S_1 manifold, (iv) from this state part of the population relaxes to ground state, S_0, radiatively, and the rest proceeds to triplet states via intersystem crossing (ISC; herein, we neglected the contribution from the relaxation to ground state through nonradiative processes), and (v) the population in the triplet states then eventually relaxes to ground state S_0.

To explain the observed photophysical behavior of the transient spectra we consider a model based on four (electronically or vibronically) excited states called S_n, S_1^*, and S_1 and the ground state S_0 connected via a sequential reaction scheme presented as photophysical model shown in Figure 10. We, then, performed global fitting using the following rate eqs 3−8 where N_0, N_1, N_2, N_3, and N_4 describe the population in S_0, S_n, S_1^*, S_1, and T_1, respectively, and gen(t) is the temporal profile of the pump pulse with 220 fs full width at half maximum (fwhm) duration.

$$\frac{dN_0(t)}{dt} = -\text{gen}(t) + \frac{k_f}{k_f + k_3}N_3(t) + k_4N_4(t) \quad (3)$$

$$\frac{dN_1(t)}{dt} = +\text{gen}(t) - k_1N_1(t) \quad (4)$$

$$\frac{dN_2(t)}{dt} = k_1N_1(t) - k_2N_2(t) \quad (5)$$

$$\frac{dN_3(t)}{dt} = k_2N_2(t) - \frac{k_3}{k_f + k_3}N_3(t) \quad (6)$$

$$\frac{dN_4(t)}{dt} = \frac{k_3}{k_f + k_3}N_3(t) - k_4N_4(t) \quad (7)$$

$$\frac{dT(t,\lambda)}{T} = S_n(\lambda)N_1(t) + S_1^*(\lambda)N_2(t) + S_1(\lambda)N_3(t) + T_1(\lambda)N_4(t) \quad (8)$$

The spectral changes, which were determined experimentally, are indicative of a continuous relaxation of the excited populations, as distinguished from a short-lived but stable intermediate. Consequently, the "basis spectra", obtained by a global fitting approach, do not represent eigen-functions on minima of the respective potential energy surface but rather represent typical magnitude of the population during their course of complete relaxation. The global fitting scheme yields the full photoinduced spectra of the excited states S_n, S_1^*, S_1, and T_1 and the estimation of rate constants k_1, k_2, and k_3. Exact interpretation of each of the rate constants is presented in Figure 11. For the fitting, we used the k_f (fluorescence rate constant) from the fluorescence lifetime data presented in our earlier reports.[32] Further, we used the triplet lifetime data from the ns-TA kinetics for the rate-constant k_4 and fixed it for fitting procedure.

Figure 12 shows the global fitting of the TA spectra recorded for Ge-TTC. The obtained basis spectra and the respective population lifetimes at each excited intermediate state brings into fore the distinction between $PIA_{singlet}$ and $PIA_{triplet}$, which were indistinguishable from the experimental observation. Notably, a closer look at the region of interest highlighted by the dotted rectangle in the left panel presents the differences in

DOI: 10.1021/acs.jpcc.5b08235
J. Phys. Chem. C 2015, 119, 28691−28700

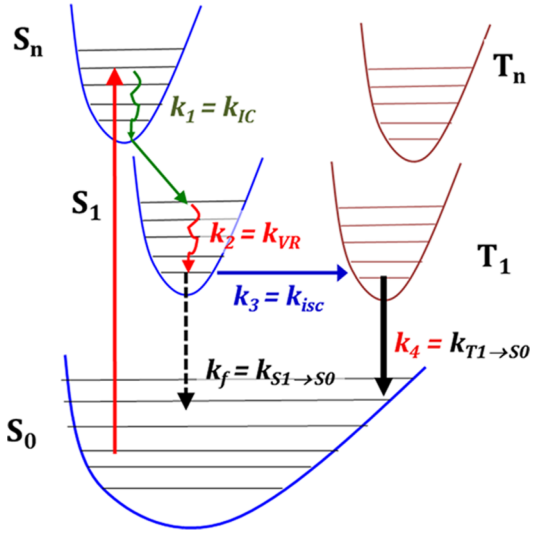

Figure 11. Schematic of the photophysical model considered for global fit analysis.

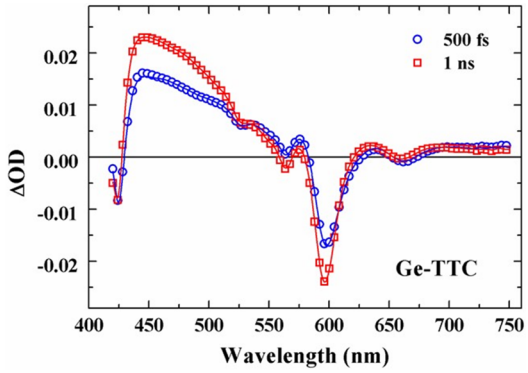

Figure 13. fs-TA spectra of Ge-TTC at a pump−probe delay of 500 fs and 1 ns demonstrating an excellent agreement of the global analysis fit (solid curve) with the experimental data (○,□).

the spectra between the vibrational hot S_1^* state and a relaxed S_1. The right panel shows the estimated population's lifetimes at each excited state. From the fitting we estimated the IC rate constant ($k_{IC} = k_1$) as 1.91×10^{12} s^{-1} corresponding to a lifetime of 525 fs, VR rate constant ($k_{VR} = k_2$) as 7.33×10^{10} s^{-1} corresponding to a lifetime of 13.6 ps, and the ISC rate ($k_{ISC} = k_3$) as 9.91×10^8 s^{-1} corresponding to a lifetime of 1.09 ns. We find an excellent agreement between the theoretical fittings and the experimental data. Figure 13 illustrates an excellent overlap of the TA spectra recorded from experiments (scatter points) and the TA spectra obtained from fitting procedures (solid line) at both extremes of the pump−probe delay (500 fs and 1 ns). The solid lines in the TA kinetics of the corroles presented in Figures 7 to 9 demonstrate a good overlap with the experimental data (scatter points). Corresponding results of global fits for the TA experiment data for TTC and P-TTC are presented in Supporting Information (Figure S6). Table 3 summarizes the photophysical parameters estimated from the global analysis of fs-TAS data for the three corroles.

CONCLUSIONS

A comprehensive photophysical investigation of three corroles TTC, P-TTC, and Ge-TTC has been performed. To achieve this we had employed TAS from femtosecond to microsecond time scales along the steady-state absorption and fluorescence spectroscopy. Using both femtosecond and nanosecond TA measurements we estimated the triplet−triplet absorption cross sections and quantum yields for all the three corroles. By performing a thorough global analysis on the obtained fs-TAS measurements we estimated rate-constants for various photophysical processes such as IC, VR, and the ISC. From our detailed analysis we conclude that Ge-TTC had superior triplet state properties compared to P-TTC and TTC. Moreover, the theoretical calculations based on TD-DFT show good agreement with the experimental absorption data. With strong extinction coefficient in the range of $(1-2.5) \times 10^5$ M^{-1} cm^{-1}, ultrafast internal conversion rates, favorable HOMO/LUMO energy levels, and excellent nonlinear optical coefficients,[32]

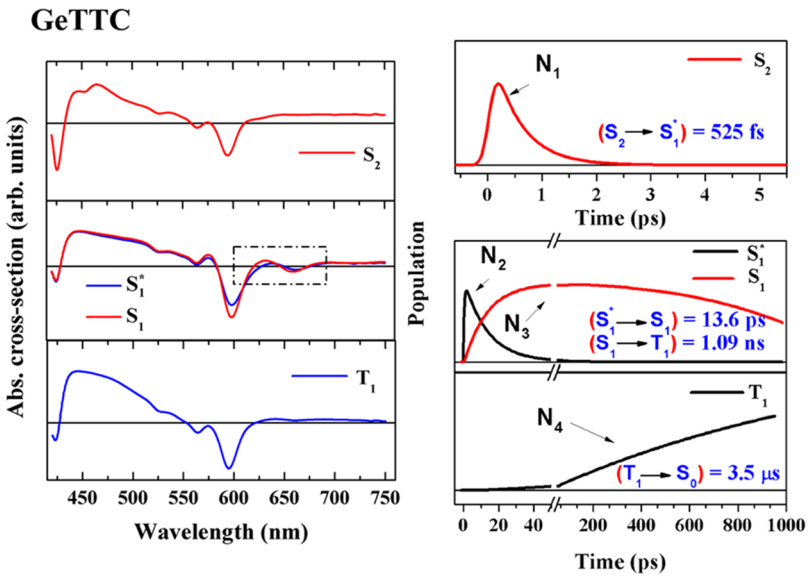

Figure 12. (left) Basis spectra for Ge-TTC obtained from the global fitting procedure. The dotted rectangle represents the spectral region where S_1^* differs from S_1; (right) the decay dynamics of different species with rate constants.

DOI: 10.1021/acs.jpcc.5b08235
J. Phys. Chem. C 2015, 119, 28691−28700

these molecules exhibit potential for various optoelectronics applications.

■ ASSOCIATED CONTENT

Supporting Information

The Supporting Information is available free of charge on the ACS Publications website at DOI: 10.1021/acs.jpcc.5b08235.

Calculated absorption spectra using TD-DFT method; femtosecond TA spectra of TTC and of P-TTC; global fitting data of TTC and P-TTC. (PDF)

■ AUTHOR INFORMATION

Corresponding Author

*E-mail: sskraavi@iith.ac.in. Phone: +91 40 23018450.

Author Contributions

The manuscript was prepared through contributions of all authors. All authors have given approval to the final version of the manuscript.

Notes

The authors declare no competing financial interest.

■ ACKNOWLEDGMENTS

R.S.S.K. thanks Dr. L. Luer, IMDEA-Madrid, for useful discussions. Authors thank Dr. A. Petrozza for extending the nanosecond-Flash Photolysis facility. Authors acknowledge J. Holt, D. Brida, and L. Luer for their contribution in software used for the data/kinetic modeling. R.S.S.K. thanks DST young scientist grant. S.V.R. thanks DRDO, India, for continued financial support. C.S. and G.L. would like to acknowledge the support of the Singapore Ministry of Education (MOE2013-T2-1-044). L.G. thanks to CSIR-XII FYP *Intel Coat* Project No. CSC-0114.

■ REFERENCES

(1) Kadish, K. M.; Smith, K. M.; Guilard, R. *The Porphyrin Handbook;* Academic Press: San Diego, CA, 2000.

(2) Tanaka, T.; Osuka, A. Conjugated Porphyrin Arrays: Synthesis, Properties and Applications for Functional Materials. *Chem. Soc. Rev.* **2015**, *44*, 943−969.

(3) Koszelewski, D.; Nowak-Krol, A.; Drobizhev, M.; Wilson, C. J.; Haley, J. E.; Cooper, T. M.; Romiszewski, J.; Gorecka, E.; Anderson, H. L.; Rebane, A.; Gryko, D. T. Synthesis and Linear and Nonlinear Optical Properties of Low-melting π-extended Porphyrins. *J. Mater. Chem. C* **2013**, *1*, 2044−2053.

(4) Jurow, M.; Schuckman, A. E.; Batteas, J. D.; Drain, C. M. Porphyrins as Molecular Electronic Components of Functional Devices. *Coord. Chem. Rev.* **2010**, *254*, 2297−2310.

(5) Guilard, R.; Barbe, J. M.; Stem, C.; Kadish, K. M. *The Porphyrin Handbook;* Kadish, K. M., Smith, K. M., Guilard, R., Eds.; Academic Press: Boston, MA, 2003; Vol *1.18*, p 303.

(6) Johnson, A. W.; Kay, I. T. 306. Corroles. Part I. Synthesis. *J. Chem. Soc.* **1965**, 1620−1628.

(7) Gross, Z.; Gray, H. B. How Do Corroles Stabilize High Valent Metals? *Comments Inorg. Chem.* **2006**, *27*, 61−72.

(8) Paolesse, R.; Jaquinod, L.; Nurco, D. J.; Mini, S.; Sagone, F.; Boschi, T.; Smith, K. M. 5,10,15-Triphenylcorrole: A Product From a Modified Rothemund Reaction. *Chem. Commun.* **1999**, 1307−1308.

(9) Gross, Z.; Galili, N.; Saltsman, I. The First Direct Synthesis of Corroles From Pyrrole. *Angew. Chem., Int. Ed.* **1999**, *38*, 1427−1429.

(10) Gross, Z. High-Valent Corrole Metal Complexes. *JBIC, J. Biol. Inorg. Chem.* **2001**, *6*, 733−738.

(11) Giribabu, L.; Sudhakar, K. Photoinduced Intramolecular Reactions in Triphenylamine−Corrole Dyads. *J. Photochem. Photobiol., A* **2015**, *296*, 11−18.

(12) Sudhakar, K.; Kanaparthi, R. K.; Kumar, Ch. K.; Giribabu, L. Synthesis and Photophysical Properties of a Novel Corrole−Anthraquinone−Corrole Molecular System. *J. Lumin.* **2014**, *153*, 34−39.

(13) Sudhakar, K.; Velkannan, V.; Giribabu, L. Synthesis, Electrochemical and Photophysical Properties of β-CarboxyTriaryl Corroles. *Tetrahedron Lett.* **2012**, *53*, 991−993.

(14) Haber, A.; Gross, Z. Catalytic Antioxidant Therapy by Metallo drugs: Lessons From Metallocorroles. *Chem. Commun.* **2015**, *51*, 5812−5827.

(15) Lai, S.-L.; Wang, L.; Yang, C.; Chan, M.-Y.; Guan, X.; Kwok, C.-C.; Che, C.-M. Gold(III) Corroles for High Performance Organic Solar Cells. *Adv. Funct. Mater.* **2014**, *24*, 4655−4665.

(16) Salvatori, P.; Amat, A.; Pastore, M.; Vitillaro, G.; Sudhakar, K.; Giribabu, L.; Soujanya, Y.; De Angelis, F. Corrole Dyes for Dye-sensitized Solar Cells: The Crucial Role of the Dye/Semiconductor Energy Level Alignment. *Comput. Theor. Chem.* **2014**, *1030*, 59−66.

(17) Walker, D.; Chappel, S.; Mahammed, A.; Brunschwig, B. S.; Winkler, J. R.; Gray, H. B.; Zaban, A.; Gross, Z. Corrole-sensitized TiO_2 Solar Cells. *J. Porphyrins Phthalocyanines* **2006**, *10*, 1259−1262.

(18) Sudhakar, K.; Giribabu, L.; Salvatori, P.; De Angelis, F. Triphenylamine-functionalized Corrole Sensitizers for Solar-Cell Applications. *Phys. Status Solidi A* **2015**, *212*, 194−202.

(19) You, L.; Shen, H.; Shi, L.; Zhang, G.-L.; Liu, H.-Y.; Wang, H.; Ji, L.-M. Photophysical Properties of the Corrole Photosensitizers. *Sci. China: Phys., Mech. Astron.* **2010**, *53*, 1491−1496.

(20) Aviv-Harel, I.; Gross, Z. Aura of Corroles. *Chem. - Eur. J.* **2009**, *15*, 8382−8394.

(21) Santos, C. I. M.; Oliveira, E.; Fernández-Lodeiro, J.; Barata, J. F. B.; Santos, S. M.; Faustino, M. A. F.; Cavaleiro, J. A. S.; Neves, M. G. P. M. S.; Lodeiro, C. Corrole and Corrole Functionalized Silica Nanoparticles as New Metal Ion Chemosensors: A Case of Silver Satellite Nanoparticles Formation. *Inorg. Chem.* **2013**, *52* (15), 8564−8572.

(22) Zhu, R.; Qiu, X.; Chen, Y.; Qian, S. Effect of Axial Substitution on the Ultrafast Dynamics and Third-order Optical Nonlinearity of Metallophthalocyanines Films. *J. Lumin.* **2006**, *119*, 522−527.

(23) Mi, J.; Guo, L.; Liu, Y.; Liu, W.; You, G.; Qian, S. Excited-state Dynamics of Magnesium Phthalocyanine Thin Film. *Phys. Lett. A* **2003**, *310*, 486−492.

(24) Kullmann, M.; Hipke, A.; Nuernberger, P.; Bruhn, T.; Götz, D. C. G.; Sekita, M.; Guldi, D. M.; Bringmann, G.; Brixner, T. Ultrafast Exciton Dynamics After Soret- or Q-band Excitation of a Directly β,β′-linked Bisporphyrin. *Phys. Chem. Chem. Phys.* **2012**, *14*, 8038−8050.

(25) Wagnert, L.; Berg, A.; Stavitski, E.; Luobeznova, I.; Gross, Z.; Levanon, H. Structure-function Relationship in Antimony Corrole Photosensitizers: Time-resolved Electron Paramagnetic Resonance and Optical Study. *J. Porphyrins Phthalocyanines* **2007**, *11*, 645−651.

(26) Rebane, A.; Drobizhev, M.; Makarov, N.; Koszarna, B.; Tasior, M.; Gryko, D. Two-Photon Absorption Properties of *meso*-Substituted A_3-Corroles. *Chem. Phys. Lett.* **2008**, *462*, 246−250.

(27) Rebane, A.; Makarov, N.; Drobizhev, M.; Koszarna, B.; Galezowski, M.; Gryko, D. T. Two-Photon Absorption Spectroscopy of Corroles. *Proc. SPIE* **2009**, *7213*, 72130Q−1.

(28) Cho, S.; Lim, J. M.; Hiroto, S.; Kim, P.; Shinokubo, H.; Osuka, A.; Kim, D. Unusual Interchromophoric Interactions in β, β′ Directly and Doubly Linked Corrole Dimers: Prohibited Electronic Communication and Abnormal Singlet Ground States. *J. Am. Chem. Soc.* **2009**, *131*, 6412−6420.

(29) Ding, T.; Aleman, E. A.; Modarelli, D. A.; Ziegler, C. J. Photophysical Properties of a Series of Free-Base Corroles. *J. Phys. Chem. A* **2005**, *109*, 7411−7417.

(30) Ventura, B.; Degli Esposti, A.; Koszarna, B.; Gryko, D.; Flamigni, L. Photophysical Characterization of Free-base Corroles, Promising Chromophores for Light Energy Conversion and Singlet Oxygen Generation. *New J. Chem.* **2005**, *29*, 1559−1566.

(31) Yang, Y.; Jones, D.; von Haimberger, T.; Linke, M.; Wagnert, L.; Berg, A.; Levanon, H.; Zacarias, A.; Mahammed, A.; Gross, Z.; Heyne, K. Assignment of Aluminum Corroles Absorption Bands to Electronic

DOI: 10.1021/acs.jpcc.5b08235
J. Phys. Chem. C 2015, 119, 28691−28700

Transitions by Femtosecond Polarization Resolved VIS-Pump IR-Probe Spectroscopy. *J. Phys. Chem. A* **2012**, *116*, 1023−1029.
(32) Anusha, P. T.; Swain, D.; Hamad, S.; Giribabu, L.; Prashant, T. S.; Tewari, S. P.; Rao, S. V. Ultrafast Excited-State Dynamics and Dispersion Studies of Third-Order Optical Nonlinearities in Novel Corroles. *J. Phys. Chem. C* **2012**, *116*, 17828−17837.
(33) Misra, R.; Kumar, R.; Prabhu Raja, V.; Chandrashekar, T. K. Modified Push−Pull Expanded Corroles: Syntheses, Structure and Nonlinear Optical Properties. *J. Photochem. Photobiol., A* **2005**, *175* (2−3), 108−117.
(34) Hamad, S.; Krishna Podagatlapalli, G.; Ahamad Mohiddon, Md.; Venugopal Rao, S. Surface Enhanced Fluorescence from Corroles and SERS Studies of Explosives Using Copper Nanostructures. *Chem. Phys. Lett.* **2015**, *621*, 171−176.
(35) Vestfrid, J.; Goldberg, I.; Gross, Z. Tuning the Photophysical and Redox Properties of Metallocorroles by Iodination. *Inorg. Chem.* **2014**, *53* (19), 10536−10542.
(36) Ngo, T. H.; Puntoriero, F.; Nastasi, F.; Robeyns, K.; Van Meervelt, L.; Campagna, S.; Dehaen, W.; Maes, W. Synthetic, Structural, and Photophysical Exploration of *meso*-Pyrimidinyl-Substituted AB_2-Corroles. *Chem. - Eur. J.* **2010**, *16*, 5691−5705.
(37) Shao, W.; Wang, H.; He, S.; Shi, L.; Peng, K.; Lin, Y.; Zhang, L.; Ji, L.; Liu, H. Photophysical Properties and Singlet Oxygen Generation of Three Sets of Halogenated Corroles. *J. Phys. Chem. B* **2012**, *116*, 14228−14234.
(38) Zhang, L.; Liu, Z.-Y.; Wang, L.-L.; Wang, H.; Liu, H.-Y.; Zhan, X. Photophysical Properties of Electron-Deficient Free-Base Corroles Bearing *meso*-Fluorophenyl Substituents. *Photochem. Photobiol. Sci.* **2015**, *14*, 953−962.
(39) Liu, X.; Mahammed, A.; Tripathy, U.; Gross, Z.; Steer, R. P. Photophysics of Soret-Excited Tetrapyrroles in Solution. III. Porphyrin Analogues: Aluminum and Gallium Corroles. *Chem. Phys. Lett.* **2008**, *459*, 113−118.
(40) Ivanova, Y. B.; Savva, V. A.; Mamardashvili, N. Z.; Starukhin, A. S.; Ngo, T. H.; Dehaen, W.; Maes, W.; Kruk, M.; Corrole, N. H. Corrole NH Tautomers: Spectral Features and Individual Protonation. *J. Phys. Chem. A* **2012**, *116*, 10683−10694.
(41) Beenken, W.; Presselt, M.; Ngo, T. H.; Dehaen, W.; Maes, W.; Kruk, M. Molecular Structures and Absorption Spectra Assignment of Corrole NH Tautomers. *J. Phys. Chem. A* **2014**, *118*, 862−871.
(42) Lemon, C. M.; Halbach, R. L.; Huynh, M.; Nocera, D. G. Photophysical Properties of β-Substituted Free-Base Corroles. *Inorg. Chem.* **2015**, *54*, 2713−2725.
(43) Flamigni, L.; Ventura, B.; Tasior, M.; Gryko, D. T. PhotophysicalProperties of a New, Stable Corrole-Porphyrin Dyad. *Inorg. Chim. Acta* **2007**, *360* (3), 803−813.
(44) Tasior, M.; Gryko, D. T.; Pielacinska, D. J.; Zanelli, A.; Flamigni, L. *Trans*-A_2B-Corroles Bearing a Coumarin Moiety - From Synthesis to Photophysics. *Chem. - Asian J.* **2010**, *5*, 130−140.
(45) Giribabu, L.; Kandhadi, J.; Kanaparthi, R. K. Phosphorus (V) Corrole-Porphyrin Based Hetero Trimers: Synthesis, Spectroscopy and Photochemistry. *J. Fluoresc.* **2014**, *24*, 569−577.
(46) Giribabu, L.; Kandhadi, J.; Kanaparthi, R. K.; Reeta, P. S. Excitational Energy and Photoinduced Electron Transfer Reactions in Ge (IV) Corrole−Porphyrin Hetero Dimers. *J. Lumin.* **2014**, *145*, 357−363.
(47) Koszarna, B.; Gryko, D. T. Efficient Synthesis of meso-Substituted Corroles in a H_2O−MeOH Mixture. *J. Org. Chem.* **2006**, *71*, 3707−3717.
(48) Kumar, R. S. S.; Lüer, L.; Polli, D.; Garbugli, M.; Lanzani, G. Primary Photo-Events in a Metastable Photomerocyanine of Spirooxazines. *Opt. Mater. Express* **2011**, *1*, 293−304.
(49) Yin, J.; Chen, R.-F.; Zhang, S.-L.; Ling, Q.-D.; Huang, W. Theoretical Studies of the Structural, Electronic, and Optical Properties of Phosphafluorenes. *J. Phys. Chem. A* **2010**, *114*, 3655−3667.
(50) Carmichael, I.; Hug, G. L. Triplet−Triplet Absorption Spectra of Organic Molecules in Condensed Phases. *J. Phys. Chem. Ref. Data* **1986**, *15*, 1−250.

DOI: 10.1021/acs.jpcc.5b08235
J. Phys. Chem. C 2015, 119, 28691−28700